Photonic band gaps in non-close-packed inverse opals

D. P. Gaillot and C. J. Summers[a)]
School of Materials Science & Engineering, Georgia Institute of Technology, Atlanta, Georgia 30332-0245

(Received 23 March 2006; accepted 19 September 2006; published online 11 December 2006)

An advanced dielectric function has been designed to compute the photonic band structures of non-close-packed inverse opals fabricated using conformal infiltration and by a recently described sacrificial-layer technique. A model is proposed to correctly simulate complex dielectric structures resulting from conformal backfilled infiltrations. While large photonic band gaps (PBGs) and a reduced refractive index requirement (RIR) are predicted to occur in these inverse structures, the results also indicate a high degree of sensitivity to the dielectric/air network topology enabling fine PBG tailoring. Optimized structurally modified non-close-packed inverse opals with lower refractive indices offer enhanced optical properties compared to narrow PBGs observed in conventional inverse shell opals using high index materials such as silicon or germanium. Three-dimensional finite-difference time-domain computations predict that many experimentally achievable non-close-packed inverse structures exhibit significantly enhanced PBG properties: a RIR as low as 2.65 and PBG width of ~10%. Additionally, a PBG width of 14.2% is predicted for an optimized high index non-close-packed inverse structure in which the interstitial air void is smaller than in structures fabricated by conformal means. The robustness and simplicity of this technique combined with predicted adjustable PBG properties is therefore demonstrated to provide alternative fabrication routes to the synthesis of photonic crystal devices operating in the visible with lower refractive indices. © *2006 American Institute of Physics*. [DOI: 10.1063/1.2396670]

I. INTRODUCTION

Three-dimensional (3D) photonic crystals (PCs) are a subclass of metamaterials that offer tremendous optical enhancements over conventional photonic devices. The predicted manipulation of the spontaneous emission rate and localization of light are a consequence of the intrinsic geometry of the structure rather than the material from which it is made.[1,2] By tailoring the nanometer scale periodicity of a high index material in one, two or three dimensions, the photonic density of states can be modified, leading to omnidirectional forbidden photonic regions or photonic band gaps (PBGs). Furthermore, engineered defects can be introduced creating defect modes within the PBG.[3] Low-threshold or thresholdless micro-emitters, ultrafast optical switches, beam steering, wave-guiding, PBG/Holey fibers and narrow-spectrum light-emitting diodes have been considered as potential photonic crystal based devices and intensively investigated.[4–10]

II. BACKGROUND

The constant progress in computation techniques to predict and tailor light properties within a PC has been driving the development of more complex fabrication techniques to synthesize structures with wider PBGs.[11–16] While two-dimensional PCs and 3D structures, such as diamond-like or woodpile structures, are commonly fabricated using "top-down" semiconductor processes,[17,18] strong constraints apply to fabricating large-scale low-cost 3D PCs.[19–21] Synthetic opals produce wide gap omnidirectional PCs[22–25] and when inverted with high refractive index materials using conformal infiltration techniques such as atomic layer deposition (ALD),[26–29] chemical vapor deposition[30–32] or other techniques,[19,33–39] produce complete PBGs as originally proposed by Busch and John.[13,14] Prior to infiltration, the air domain comprises tetrahedral and octahedral air sites, as shown in Fig. 1(a). With increasing conformal infiltration the air channels eventually close at 86% of the air interstitial volume. This prevents further infiltration and leaves the backbone sandwiched between disconnected air lattices trapped within the backbone and the fcc air lattice resulting from the removal of the original opal template. As we have shown previously, highly conformal silicon inverse shell opals exhibit a direct PBG between the eighth and ninth bands at the W point, provided the refractive index n exceeds

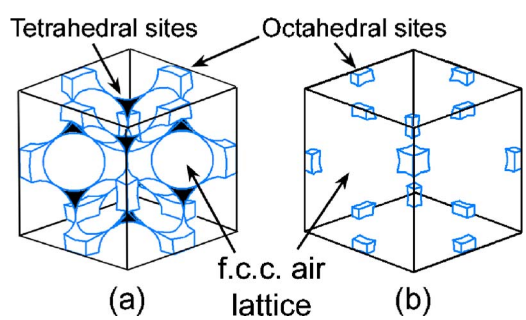

FIG. 1. (Color online) (a) Air network introduced in an inverse shell opal in which 86% of the interstitial space is conformally infiltrated. Tetrahedral sites are shaded. (b) Air network introduced in an inverse shell opals in which 97.2% of the interstitial air space is conformally infiltrated. The remaining octahedral air sites define a disconnected fcc lattice which is displaced by half a unit cell from the main fcc network.

a)Electronic mail: chris.summers@mse.gatech.edu

3.3.[40] The high refractive index requirement (RIR) limits the PBG width from 2.5% to 9.2% for $n \sim 3.45$ to 4.0, thereby restricting operation to the IR.

By sintering an opal template, the main fcc air lattice becomes highly connected by circular interconnections formed by the sphere overlap, as the lattice constant is decreased[13,14] resulting in a non-close-packed fcc lattice with enhanced PBG properties.[31,41] In 2000, Doosje *et al.* predicted a 10% PBG in a fully infiltrated silicon non-close-packed inverse opal,[41] Later, the Fenollosa and Garcia-Santamaria groups,[42–44] demonstrated selective chemical etching and nanorobotic manipulation, respectively, to achieve templates for non-close-packed inverse structures. In 2003, Míguez *et al.* fabricated non-close-packed inverse structures by conformal backfilling silicon into a silica micromold[31,41] and produced a wide range of structures exhibiting complete PBGs. Recently, we reported an ALD technique whereby a silica template was presintered, infiltrated with TiO_2,[45] and after removal of the sintered template, conformally backfilled with TiO_2, resulting in a non-close-packed inverse opal. However, despite these titania structures exhibiting larger pseudo-PBGs, sintering provided insufficient modification and control over the original template to further increase the PBG and resulted in thin-film cracking.

To overcome these limitations, a modified non-close-packed fabrication scheme using atomic layer deposition was developed by Graugnard *et al.* involving the deposition of conformal multiple layered materials.[46] With this technique, structural modifications to the original template and inverse shell opal backbone can be made with precise and independent control of the tube and sphere radii, adding additional geometrical flexibility and PBG adjustment. In this technique (Fig. 2), a synthetic opal is conformally and sequentially infiltrated with a buffer material (that can be selectively etched and which therefore acts as a sacrificial buffer layer), resulting in an overlapping template, as shown in Fig. 2(a). A high refractive index material is then infiltrated into the remaining air void up to the maximum conformal infiltration, as depicted in Fig. 2(b). After selective removal of the modified template [original opal and sacrificial shell; Fig. 2(c)], a low-filling-fraction inverse shell structure is formed [Fig. 2(d)], which becomes a backbone template for further structural manipulation. The sacrificial-layer technique mimics the sintering process, by providing a mechanism whereby air pores, of radius R_c, can be formed and finely engineered since their width is geometrically related to the outer sacrificial shell radius (or inner radius of the backbone template), as the inset of Fig. 2 indicates. Finally, this backbone template can be further modified by conformally coating dielectric layers onto its interior, as reported by Míguez *et al.*, King *et al.*, and Graugnard *et al.*,[31,45,46] and shown in Fig. 2(e). As illustrated in Fig. 2, as conformal backfilling increases, the air pore radius decreases and hyperboloid channels form rather than perfectly tubular channels. The introduction of a sacrificial shell coupled with conformal backfilling adds significantly more flexibility to geometrical manipulation, allowing fabrication of many inverse structures exhibiting different PBG properties. Since the outer radius of the backbone template R_{shell} is defined by the point of maximum

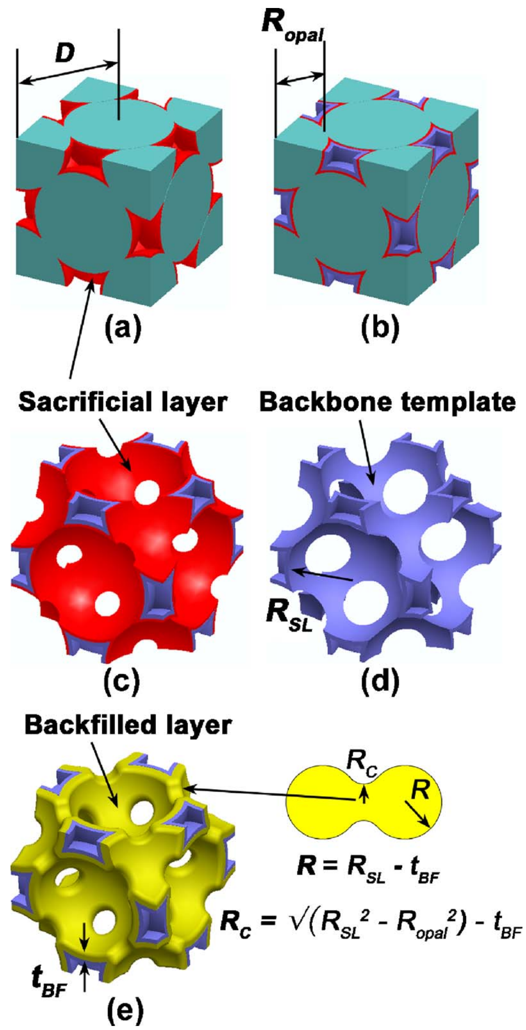

FIG. 2. (Color online) Sacrificial-layer process used to synthesize non-close-packed inverse shell opals. (a) Bare opal is conformally infiltrated with a sacrificial shell of radius R_{SL}. (b) High index material is then infiltrated onto the sacrificial layer up to the maximum infiltration of 86% ($R_{shell}/D = 0.5775$). (c) Original template is removed, leaving a multilayer inverse opal. (d) Sacrificial layer is removed, forming a lattice of overlapping air spheres within a dielectric backbone. (e) The backbone is then conformally backfilled to yield the desired structure. This leads to hyperboloid connections between the spherical air domains, as shown in the bottom right inset.

86% conformal infiltration, two design parameters define the resulting structure: the sacrificial shell radius R_{SL}, and the conformal backfilling thickness t_{BF}.

We present here a dielectric model that enables photonic band computations of structurally modified non-close-packed inverse shell opals fabricated by the conformal sacrificial-layer/backfilling technique. The PBG width and RIR dependence on R_{SL} and t_{BF} were theoretically investigated using 3D finite-difference time-domain simulations (3D-FDTD). In addition, we have investigated network topologies in which the outer radius of the backbone template exceeds the practical case of maximum conformal infiltration and the properties of the inverse "tube-like" structure reported by Doosje *et al.*, and in which tetrahedral and octahedral air pockets were introduced.

From this study, we demonstrate non-close-packed inverse structures with large PBGs and reduced RIR. We also show that these properties can be tailored by varying the fabrication parameters. The simplicity and robustness of a sacrificial-layer technique potentially enables opal-based PCs exhibiting wide PBG widths and reduced RIR ($n \geq 2.65$) operating in the visible region. Additionally, it is shown that the PBG mechanism is controlled by the eighth band at the *W* point and is strongly dependent on the conformal backfilling infiltration.

III. SIMULATIONS

In this work, the PBGs and the RIR of specific structures were computed using a 3D-FDTD technique, which is a powerful tool to compute photonic band structures of complex dielectric functions such as 3D PCs.[11,12,47] In the 3D-FDTD technique, modes that are allowed within the PC are extracted for each *k*-point from the power spectrum generated after fast Fourier transform operations on stored random fields. The allowed frequencies are normalized with respect to the PC geometry ($\omega_n = a/\lambda$, where a is the cubic lattice constant). The code then moves to the next *k*-point, where the same protocol is repeated. The allowed frequencies versus *k*-vector are then plotted to form the photonic band diagram.

A dielectric model that simulates a sacrificial shell and subsequent conformal backfilling infiltration was developed. The final unit cell ($50 \times 50 \times 50$ grid resolution) was reconstructed as an averaged dielectric function from a larger unit cell with a higher grid resolution ($250 \times 250 \times 250$ for one-eighth of a unit cell) to avoid abrupt changes in dielectric values ("staircase" effect). Typically, this was performed by averaging the fine mesh with 10 subcells. In order to assess the proficiency of the numerical grid (convergence and time), computations of an inverse shell opal presenting a known complete PBG were performed by using meshes with $50 \times 50 \times 50$, $70 \times 70 \times 70$, and $150 \times 150 \times 150$ points per unit cell. The grid size resolution, given by the ratio of the lattice constant ($a = \sqrt{2}D$) to the grid size, is then $0.0283D$, $0.0202D$, and $0.0094D$, respectively. The Bragg peak width obtained with the higher resolution grid was $\sim 4\%$ greater than with the coarse grid ($\sim 2\%$ between the coarse and intermediate case). Furthermore, the code using a finer grid size of 150 takes 24 times longer than a coarse grid size of 50 and uses 80 times more memory. Similarly, the intermediate case of 70 points per unit cell takes 11 times longer and 10 times more memory. This indicates that a grid size of 50 yields sufficient convergence while preserving simulation time and memory. As a consequence, since the thickness of the coated layers used in this work is above $0.01D$, a $50 \times 50 \times 50$ cubic grid was chosen to ensure reliable convergence.

First, sacrificial layers were applied to the original opal template as a function of the coated sphere radius R_{SL} to the opal sphere diameter D, which defines the inner dielectric shell radius prior to conformal backfilling. As previously mentioned, the maximum allowed infiltration for conformal coverage is 86% of the interstitial air volume ($R_{shell}/D = 0.5775$) so that the sacrificial shell radius R_{SL}/D can vary from values greater than 0.5 (the conventional close-packed structure) up to radii slightly lower than 0.5775, the limit on the radius imposed by the conformal coating geometry. The conformal backfilling infiltration was then modeled using a numerical algorithm. In this algorithm, the conformal backfilling thickness t_{BF} was defined as a ratio to the original sphere diameter D. The code then searched for the shell/air interfaces (the dielectric shell is defined by "ones" and the air by "zeros"), at which point a sphere with a radius of 4 mesh units was created with "ones" (dielectric material). This procedure is repeated until reaching the desired backfilling thickness. The accuracy of the conformal backfilling infiltration model is therefore a function of the deposited sphere radius which has to be as small as possible compared to the main grid size. In this work, the deposited sphere radius of 4 mesh units corresponds to a thickness of $0.0138D$. Although the numerical grid size of the averaged dielectric function is $0.028D$, our simulations indicate that the averaging process preserves well the original template. The bands were observed to shift for templates whose fabrication parameter values deviate only by $0.0002D$. This validates the four-digit resolution used for the sacrificial shell radii (R_{SL}/D), the outer radii of the backbone template (R_{shell}/D) and conformal backfilling thicknesses (t_{BF}/D). In a typical 500 nm lattice constant opal, this resolution equals a 0.1 nm growth of a dielectric material (0.0002×500 nm $= 0.1$ nm). This closely matches the dielectric growth rate per cycle in an opal reported by King *et al.*,[29] of about 0.05 nm (fabrication resolution) for ALD of TiO_2. Additionally, as dielectric material is deposited and conforms to the shape of the inside of the backbone, the width of the formed hyperboloid channels decreases and eventually closes, preventing more material from being added.

Figure 3(a) presents the cross section through the [100] plane demonstrating the parameterization of an non-close-

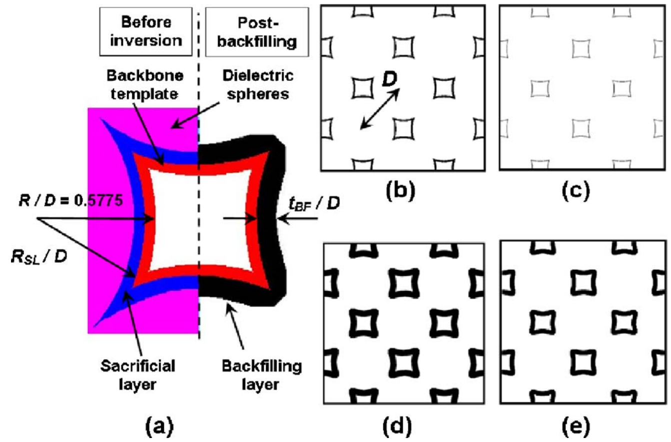

FIG. 3. (Color online) (a) Cross section through the [100] plane to demonstrate parameterization scheme used to define non-close-packed inverse shell dielectric functions. (b) and (c) depict schematic cross-sections of backbone templates prior to conformal backfilling, in which the backbone outer radius is $R_{shell}/D = 0.5775$ (86% of the air interstitial space infiltrated), while (d) and (e), respectively, depict the cross sections of a resulting non-close-packed inverse opal after a $0.083D$ conformal backfilling infiltration. (b) [100] top view of an inverse shell opal using an etched sacrificial shell radius of $0.5462D$. (c) [100] top view of an inverse shell opal using a sacrificial shell radius of $0.5693D$. (d) and (e) show that final structures present different spheres and hyperboloid channels sizes depending upon the sacrificial shell radius.

packed inverse opal dielectric function. Figures 3(b) and 3(c) show the schematic cross sections of overlapping inverse shell structures using two different sacrificial shell radii, and Figs. 3(d) and 3(e) show the final structures after conformal backfilling with the same thickness. As the conformal backfilling thickness increases, hyperboloid channels form. Their width is controlled by the original sacrificial shell radius and the conformal backfilling thickness, thus demonstrating the potential of the model. In addition, the backbone outer radius (R_{shell}/D) can be increased to modify the trapped air lattices and study its influence on the PBG properties.

IV. RESULTS AND DISCUSSION

In this section, we first present the PBG properties: complete PBG width and refractive index requirement (RIR) of experimentally achievable high index non-close-packed inverse shell opals ($n=3.45$) fabricated using the sacrificial-layer and conformal backfilling processes. We then extend the investigations to structures whose outer radius exceeds the 86% infiltration maximum allowed for conformal coatings. Finally, we present the PBG properties of high index inverse "tube-like" non-close-packed structures (based on Doosje's optimized network topology), in which geometrically defined air pockets are introduced within the backbone.

A. High index non-close-packed inverse shell opals

1. Experimentally achievable 86% non-close-packed inverse structures ($R_{shell}/D=0.5775$)

In this fabrication scheme, the backbone is grown conformally on top of the sacrificial shell to the allowed maximum radius of $R_{shell}/D=0.5775$, similar to inverse shell opals. After proper removal of the original dielectric sphere template and sacrificial layers, thus leaving a conformal backbone template, the structure is then conformally backfilled and the generated dielectric function is used to perform band structure calculations. Since two fabrication parameters—the sacrificial shell radius and conformal backfilling thickness—now define the resulting structure, a systematic approach was used to sample the large number of structures one could possibly fabricate. Values for the sacrificial shell radius R_{SL} and conformal backfilling thickness t_{BF} were then selectively chosen within their respective boundaries to limit computation time. The maximum conformal backfilling thickness t_{BF}/D that can be achieved is given by

$$t_{BF}/D = \sqrt{(R_{SL}/D)^2 - (R_{opal}/D)^2}. \quad (1)$$

It follows from Eq. (1) that t_{BF}/D varies from values slightly higher than zero to values slightly lower than 0.289 (0.5775/2), respectively, for a sacrificial-shell radius just slightly higher than $R_{SL}/D=0.5$ and slightly lower than $R_{SL}/D=0.5775$; $R_{opal}/D=0.5$ for a close-packed geometry.

In order to investigate the PBG properties, it is convenient to plot the evolution of the normalized frequency at the lower and upper edges of the bands defining the complete PBG as a function of the fabrication parameters: sacrificial shell radius R_{shell}/D, and conformal backfilling thickness t_{BF}/D. The behavior of the edges and gap width can be monitored as a function of the fabrication parameters and related to the underlying mechanisms responsible for the complex behavior of a complete PBG. Additionally, by taking the frequency difference $\Delta\omega$ between the upper and lower edge of the gap and dividing by the midgap frequency ω_0, one can obtain the gap width ratio, defined as $\Delta\omega/\omega_0$. It follows that such a chart can be used to predict whether structures exhibit a complete PBG or not, and how static adjustments of the network topology affect the PBG width and peak location.

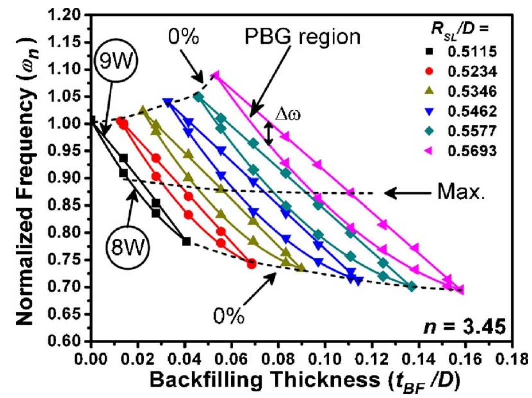

FIG. 4. (Color online) Evolution of the band edges defining the eighth-ninth PBG for a normalized frequency ω_n as a function of conformal backfilling thickness t_{BF}/D for high index structures formed using a $R_{shell}/D=0.5775$ backbone outer radius and sacrificial-shell radius values varying from $R_{SL}/D=0.5115$ to 0.5693. The region comprised between the lower and upper W bands indicates structures for which a complete PBG was predicted. The upper, lower, and central dashed lines indicate locations at which the PBG opens, closes, and is maximum, respectively.

Figure 4 shows the evolution of the normalized frequencies ($\omega=\sqrt{2}D/\lambda$) of the upper edge of the eighth band and lower edge of the ninth band as a function of conformal backfilling thickness for structurally normalized values (t_{BF}/D) ranging from 0.0138 to 0.194 and sacrificial shell radius (R_{SL}/D) for values ranging from 0.5115 to 0.5693. The corresponding infiltrated dielectric volume of the sacrificial material ranges from 18.3% to 81.9% of the interstitial air voids. Figure 4 indicates that 86% infiltrated non-close-packed inverse opals exhibit a direct PBG between the eighth and ninth bands at the W point; the complete gap region being bounded by the lower and upper curves in this figure. Thus, Fig. 4 demonstrates that, as the backfilling thickness was increased and for any sacrificial-shell radius values, the upper edge of the PBG decreased linearly, whereas the lower edge decreased parabolically. As a consequence, the eighth band at the W point strongly affects the behavior of the PBG as the backfilling thickness is increased, and there exist three critical backfilled thickness values resulting in structures in which a complete direct PBG is formed, a maximum direct PBG is predicted, and the PBG is closed. The upper and lower dashed lines indicate the location at which the eighth and ninth bands intersect, thus resulting in an opened or closed PBG. The central dashed line indicates the location at which the maximum PBG width is obtained for each structure. From a geometrical point of view, as the conformal backfilling thickness is increased, it would be assumed that the electromagnetic field power density in the dielectric band

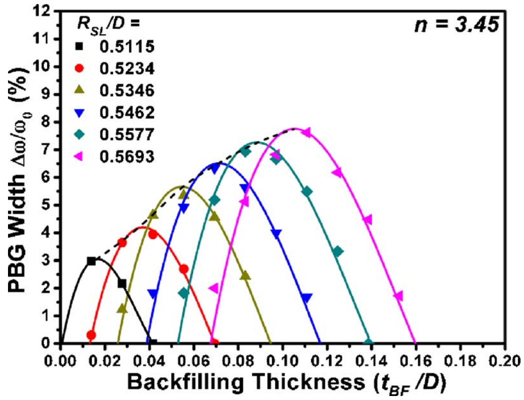

FIG. 5. (Color online) Evolution of the PBG ($\Delta\omega/\omega_0$ in percent) as a function of conformal backfilling thickness (t_{BF}/D) for sacrificial-shell radius values (R_{SL}/D) varying from 0.5115 to 0.5693 (maximum conformal backfilling thickness varies from 0.1078D to 0.2722D, respectively). The outer radius of the resulting high index structures is $R_{shell}/D=0.5775$ corresponding to an 86% maximum infiltration of the interstitial air space. The dashed line depicts the locus of the maximum PBG observed for a given sacrificial-shell radius.

mode (i.e., the lower PBG band) would increase and concentrate in the thicker dielectric backbone. Similarly, the electromagnetic field power density in the air band mode (i.e., the upper PBG band) would decrease due to the decreasing air sphere and tube filling fraction. Since the dielectric contrast between the backbone material and air favors a significantly larger electromagnetic field density in the dielectric regions, this allows the degeneracy at the W point to be lifted and a gap is formed which increases with backfilling. This also implies that the shift in the dielectric band with backfilling thickness is accrued compared to that of the air band. In contrast, very thick backfilled dielectric layers modify the architecture so that the air/dielectric network topology is altered resulting in a more pronounced non-close-packed structure. The air tube connections become highly filled and the interaction of the thicker dielectric shell surrounding the air tube is believed to allow the electromagnetic field to be redistributed from the dielectric to the air domains. This redistribution mechanism compensates for the decrease in filling fraction and electromagnetic power density in the air domains. It follows that the dielectric band shift is then slowed down by the backfilling process, whereas the air band shift remains linear. Under these conditions, it is shown in Fig. 4 that the gap eventually closes.

Figure 5 shows the evolution of the complete PBG width between the eighth and ninth bands obtained from Fig. 4, i.e., $\Delta\omega/\omega_0$, as a function of the fabrication parameters. Due to the behavior discussed above, this results in symmetrical ($\Delta\omega/\omega_0$ vs t_{BF}/D) curves centered around the maximum PBG width value. Figures 4 and 5 indicate that as the sacrificial-shell radius is increased, resulting in a thinner backbone template with wider air pores, larger PBGs are obtained after subsequent conformal backfilling infiltration into the interior of the backbone. Accordingly, the gap region expands; providing an increasing number of structures with complete and direct PBGs, as shown in Fig. 5. These figures indicate that, as the sacrificial-shell radius is increased, a thicker, conformally backfilled layer is required to open a PBG. In fact, a structure resulting from the backfilling of the thinnest backbone template yields the largest PBG width and widest PBG region. The locus of the maximum PBGs obtained for structures fabricated with different sacrificial-shell radii, and indicated by the dashed line in Fig. 5, shows that a maximum PBG width of 7.62% is predicted for a structure with a sacrificial-shell radius of $R_{SL}/D=0.5693$ and conformal backfilling thickness of $t_{BF}/D=0.1108$ (corresponding to $\sim$40% of maximum conformal backfill infiltration). This PBG value is approximately three times larger than that predicted by Busch and John for a silicon inverse shell opal ($\sim$2.5%).[13,14] Remarkably, the maximum PBG width at any given sacrificial shell radius was found to occur for a dielectric filling fraction of $\sim$30%; a value also observed for theoretical diamond structures, which are predicted to exhibit the highest PBG values.[11] In our previous work,[40] it was reported that inverse shell opals fabricated using conformal infiltration techniques exhibit a direct gap. It was also predicted that a similar architecture with a higher filling fraction would favor the formation of a larger PBG. This is confirmed in the present work.

Additionally, Fig. 4 shows that as the sacrificial shell radius is increased, resulting in a thinner backbone template with wider air pores, the midgap frequency difference between the structures in which a complete gap is predicted to open and close, increases. This strongly indicates that PBG width and peak location can be adjusted in non-close-packed inverse structures by selectively choosing the conformal backfilling thickness, which is easily performed using ALD.[46] As the conformal backfilling thickness is increased, the dielectric filling fraction rapidly increases and consequently, the 8-9 midgap shifts down in frequency. The according wavelength increases and spans a large spectrum. More importantly, when coupled with a large sacrificial-shell radius, the PBG can be adjusted to operate at any desired wavelength. However, in order to maintain the mechanical stability of the backbone template after inversion, a smaller sphere radius has to be used which restricts the sacrificial-layer radius and the formation of a complete PBG at a lower wavelength region.

2. Theoretical non-close-packed inverse shell structures ($0.5775<R_{shell}/D<0.707$)

Busch and John reported enhanced PBG properties for an inverse shell opal in which the outer shell radius can exceed the 86% infiltration maximum for conformal coatings. Similarly, it is suggested in our work that non-close-packed inverse shell structures with an outer radius larger than $R_{shell}/D=0.5775$ would present enhanced PBG properties. However, in this particular scheme, three fabrication parameters are now required to define the theoretical non-close-packed inverse shell structure: sacrificial shell radius R_{SL}/D, conformal backfilling thickness t_{BF}/D, and the addition of the outer radius of the backbone template R_{shell}/D. In order to reduce the large number of structures that can be modeled, the values of the sacrificial shell radii were chosen from the previous study that predicted the best PBG properties, as summarized in Figs. 4 and 5: $R_{SL}/D=0.5462$ (63.2% infiltrated air volume), 0.5577 (73.6% infiltrated air volume),

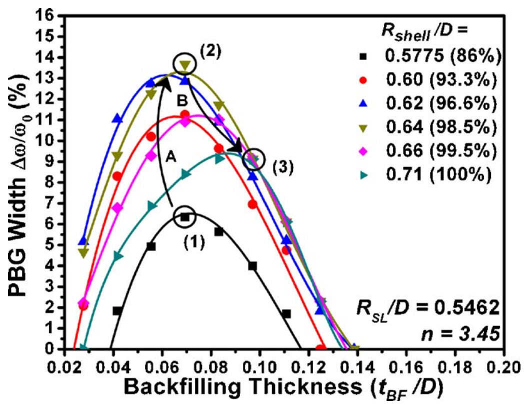

FIG. 6. (Color online) Evolution of the PBG ($\Delta\omega/\omega_0$ in percent) as a function of conformal backfilling thickness (t_{BF}/D) for values ranging from 0.014 to 0.138 and backbone outer radius R_{shell}/D for values ranging from 0.5775 to 0.707 in high index non-close-packed inverse shell structures with a $R_{SL}/D=0.5462$ sacrificial shell radius. A 13.7% PBG width is predicted for a structure with a outer radius $R_{shell}/D=0.64$ and a conformal backfilling thickness $t_{BF}/D=0.069$.

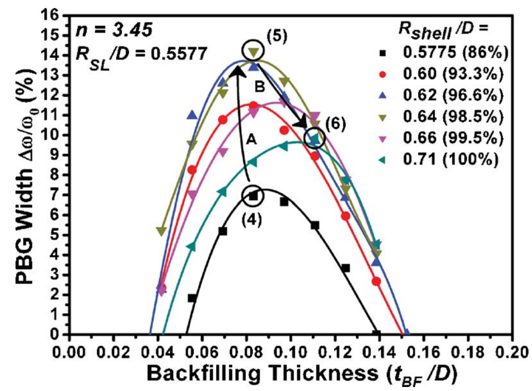

FIG. 7. (Color online) Evolution of the PBG width ($\Delta\omega/\omega_0$ in percent) as a function of conformal backfilling thickness (t_{BF}/D) for values ranging from 0.041 to 0.167 and backbone outer radius R_{shell}/D for values ranging from 0.5775 to 0.707 in high index non-close-packed inverse shell structures with a $R_{SL}/D=0.5577$ sacrificial-shell radius. A 14.2% PBG width is predicted for a structure with a outer radius $R_{shell}/D=0.64$ and a conformal backfilling thickness $t_{BF}/D=0.083$.

and 0.5693 (81.9% infiltrated air volume). The PBG width was then computed for high index infiltration ($n=3.45$) and for backbone template outer radius values varying from $R_{shell}/D=0.5775$ to 0.707 (86% to 100% infiltrated air volume) and as a function of the conformal backfilling thickness for values varying from $t_{BF}/D=0.014$ to 0.1663, corresponding to ~60% of the maximum conformal backfilling infiltration.

Figure 6 shows the PBG width as a function of the backbone outer radius R_{shell}/D and conformal backfilling thickness t_{BF}/D for structures fabricated using a sacrificial-shell radius of $R_{SL}/D=0.5462$ (63.2% infiltrated air volume). This figure indicates that as the conformally backfilled thickness increased, and for any sacrificial-layer radii, the complete PBG width first increased, reached a maximum value, and then decreased to zero. This figure also shows that structures with outer radius backbone values varying from $R_{shell}/D=0.5775$ to 0.64 (98.5% infiltrated air volume) are predicted to exhibit a maximum PBG width for a conformal backfilling thickness of $t_{BF}/D\sim0.0693$. Additionally, the maximum PBG width increases with the outer radius of the backbone. The predicted direct $W-W$ gap behavior is controlled by the mechanism discussed in the previous paragraph. However, as the backbone outer radius increased from $R_{shell}/D=0.64$ to 0.707 (100% infiltrated air volume), the predicted maximum PBG width decreases, thus requiring thicker conformally backfilled layers. In contrast, these structures are predicted to exhibit an indirect $W-X$ gap.[40] As the structure approaches the direct/indirect PBG transition ($R_{shell}/D=0.64$), the frequency of the upper band at the X point (air mode) is abruptly pulled down to cross the ninth band at the W point to form an indirect PBG. This is because the octahedral air sites can no longer sustain a high electromagnetic field power density and a slight increase in the infiltration promotes a large transfer of the electromagnetic field power density to the backbone, which pushes the X point frequency down at a higher rate. The bold line in Fig. 6 depicts the locus of the maximum PBG width as a function of the backbone outer radius and conformal backfilling thickness. The A and B sections of the locus identify structures in which the PBG is defined by direct ($W-W$) and indirect ($W-X$) gap structures, respectively.

Figure 7 shows PBG width computations as a function of the backbone outer radius R_{shell}/D and conformal backfilling thickness t_{BF}/D for structures fabricated using a sacrificial shell radius of $R_{SL}/D=0.5577$ (73.6% infiltrated air volume). As this figure indicates, the behavior of the PBG follows a trend similar to the PBG predicted for structures fabricated using a $R_{SL}/D=0.5462$ sacrificial-shell radius (63.2% infiltrated air volume) and shown in Fig. 6. The maximum PBG widths are slightly higher as compared to equivalent structures fabricated using a smaller sacrificial-shell radius, as shown in Figs. 5 and 6. In addition, this figure shows that structures with outer radii varying from $R_{shell}/D=0.5775$ to 0.64 (98.5% infiltrated air volume) are predicted to exhibit a maximum direct $W-W$ PBG width for conformal backfilling thickness of $t_{BF}/D\sim0.083$. Again, as the backbone outer radius was increased from $R_{shell}/D=0.64$ to 0.707 (100% infiltrated air volume), the predicted maximum indirect $W-X$ PBG width decreases, thus requiring thicker conformally backfilled layers. The bold line in Fig. 7 depicts the locus of the maximum PBG width as a function of the backbone outer radius and conformal backfilling thickness. The A and B sections of the locus identify structures in which the PBG is defined by a direct $W-W$ gap and an indirect $W-X$ gap, respectively.

Finally, Fig. 8 shows PBG width computations performed for the largest sacrificial-shell radius investigated of $R_{SL}/D=0.5693$ (81.9% infiltrated air volume). As indicated, the PBG follows a similar trend to those shown in Figs. 6 and 7. Again, the maximum PBG widths are slightly higher as compared to equivalent structures fabricated using a smaller sacrificial shell radius. The data also show that structures with outer radii varying from $R_{shell}/D=0.5775$ to 0.64 (98.5% infiltrated air volume) are predicted to exhibit a maximum direct $W-W$ PBG width for conformally backfilled thickness of $t_{BF}/D\sim0.1108$. Again, as the backbone outer radius is increased from $R_{shell}/D=0.64$ to 0.707 (100%

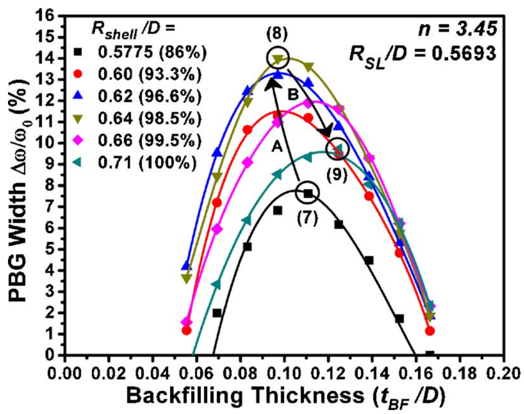

FIG. 8. (Color online) Evolution of the PBG width ($\Delta\omega/\omega_0$ in percent) as a function of conformal backfilling thickness t_{BF}/D for values ranging from 0.055 to 0.167 and backbone outer radius R_{shell}/D for values ranging from 0.5775 to 0.707 in high index non-close-packed inverse shell structures with a $R_{\mathrm{SL}}/D=0.5693$ sacrificial-shell radius. A 14% PBG width is predicted for a structure with a outer radius $R_{\mathrm{shell}}/D=0.64$ and a conformal backfilling thickness $t_{\mathrm{BF}}/D=0.097$.

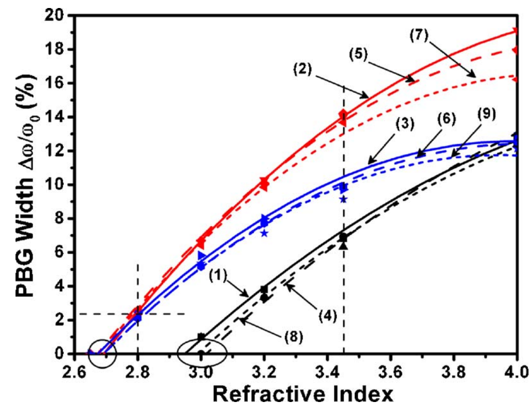

FIG. 9. (Color online) Evolution of PBG ($\Delta\omega/\omega_0$ in percent) as a function of refractive index for structures 1 to 9 circled in Figs. 6–8, and defined by three structural groups. The first structural group comprises 86% inverse non-close-packed shell opals that are experimentally achievable using conformal sacrificial-layer/backfilling infiltration steps ($R_{\mathrm{shell}}/D=0.5775$), and were predicted to exhibit a maximum direct $W-W$ PBG width. The second structural group comprises non-close-packed inverse shell opals whose outer radius $R_{\mathrm{shell}}/D=0.64$, greater than the 86% maximum infiltration possible with conformal infiltration, were predicted to exhibit a maximum direct/indirect $W-W/W-X$ PBG width. The last structural group comprises similar non-close-packed inverse opals in which no air pockets are present within the backbone ($R_{\mathrm{shell}}/D=0.707$) and were predicted to exhibit a maximum indirect $W-X$ PBG width.

infiltrated air volume), the predicted maximum indirect $W-X$ PBG width decreases, thus requiring thicker conformally backfilled layers. Similar to Figs. 6 and 7 the bold line in Fig. 8 depicts the locus of the maximum PBG width as a function of backbone outer radius and conformally backfilled thickness, and the A and B sections of the locus identify structures in which the PBG is defined by a direct $W-W$ gap and an indirect $W-X$ gap, respectively.

These calculations predict that a high index non-close-packed inverse structure fabricated using a $R_{\mathrm{SL}}/D=0.5577$ sacrificial shell radius (73.6% infiltrated air volume), a $R_{\mathrm{shell}}/D=0.64$ backbone outer radius (98.5% infiltrated air volume), and a $t_{\mathrm{BF}}/D=0.083$ conformally backfilled thickness yields a 14.2% PBG width. For comparison, the highest PBG width predicted before this work was ~10.3% in 97.2% infiltrated silicon inverse shell opals.[13,14,40] The extension of these calculations to inverse opal structures with a $R_{\mathrm{shell}}/D=0.707$ outer radius (100% infiltration), a $R_{\mathrm{SL}}/D=0.5577$ sacrificial shell radius (73.6% infiltrated air volume) and a $t_{\mathrm{BF}}/D=0.1247$ conformally backfilled thickness yields a 9.83% PBG width, close to the maximum value of 9.59% reported by Doosje *et al.* for their optimized structure.

The structures fabricated using a sacrificial shell radius of $R_{\mathrm{SL}}/D=0.5462$, $R_{\mathrm{SL}}/D=0.5577$, and $R_{\mathrm{SL}}/D=0.5693$, respectively, and exhibiting the largest PBG widths were grouped into three structural types to study the influence of structural modifications on the refractive index requirement (RIR). All of these structures were numbered from 1 to 9, and are circled in Figs. 6–8 for clarity. These structural types present dielectric/air network topologies that are dominated by different PBG mechanisms and behaviors, as discussed earlier. The first structural type comprises 86% non-close-packed inverse shell opals that are experimentally achievable using conformal sacrificial-layer/backfilling and in which an optimized conformally backfilled thickness results in a maximum direct $W-W$ PBG width. For this group, structures 1, 4, and 7 were defined using a $R_{\mathrm{shell}}/D=0.5775$ backbone outer radius. In contrast, the second structural type comprises non-close-packed inverse shell opals whose outer radius is greater than the 86% maximum infiltration possible with conformal infiltration, and were predicted to exhibit a maximum direct/indirect $W-W/W-X$ PBG width. For this group, structures 2, 5, and 8 were defined using a $R_{\mathrm{shell}}/D=0.64$ backbone outer radius. The last structural type comprises similar non-close-packed inverse opals in which no air pockets are present within the backbone and were predicted to exhibit a maximum indirect $W-X$ PBG width. Finally, for this group, structures 3, 6, and 9 were defined using a $R_{\mathrm{shell}}/D=0.707$ backbone outer radius. The summary of the RIR computed for these nine structures is presented in Fig. 9 for refractive index values varying from 2.6 to 4.0. The data show that the 86% infiltrated non-close-packed inverse shell structures, i.e., 1 to 3, exhibit a complete PBG for refractive indices greater than 2.9 compared to 3.3 for the more conventional 86% infiltrated inverse shell opals. This is despite the fact that structures 1 to 3 were fabricated using different combinations of sacrificial-shell radii (respectively, $R_{\mathrm{SL}}/D=0.5462$, 0.5577, and 0.5693; corresponding to 63.2%, 73.6%, and 81.9% infiltrated air volumes) and conformally backfilled thicknesses (respectively $t_{\mathrm{BF}}/D=0.069$, 0.083, and 0.1108). A RIR as low as 2.65 was found in structures 4 to 6, presenting the maximum PBG width for backbone outer radii $R_{\mathrm{shell}}/D=0.64$, which was also found for the fully infiltrated structures ($R_{\mathrm{shell}}/D=0.707$) 7 to 9. To the authors' knowledge, this value is also the lowest RIR ever reported in opal-based photonic crystals to date. All the PBG properties presented in the previous paragraphs strongly demonstrate the potential of the sacrificial-layer technique coupled with a conformal infiltration technique. This process offers greater control and flexibility to the architecture design of non-close-packed inverse shell opals. More importantly, it provides precise adjustment of the PBG properties to obtain larger PBG widths and reduced RIR. Furthermore, theoretical results

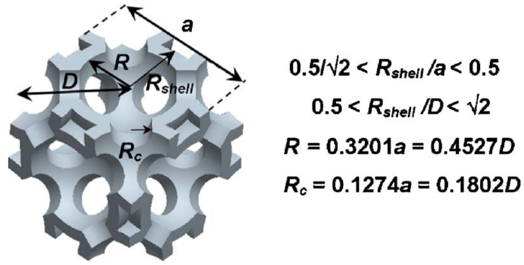

FIG. 10. (Color online) Unit cell of a non-close-packed inverse shell tube-like structure. The main air network is a replica of the Doosje inverse structure presented in Fig. 2. Air pockets as presented in Fig. 1(a) are introduced within the backbone.

also indicate unprecedented properties for fully infiltrated non-close-packed inverse structures. By combining a conformal infiltration technique with a sol/gel technique, for example, one should be able to fabricate a structure with a RIR as low as 2.65, which enables PBG operation in the visible with optically transparent materials such as TiO_2.

B. High index inverse shell "tube-like" non-close-packed opals

In addition to the above, we also investigated the influence of modified air pockets on the PBG width and RIR in the tube-like high index structure proposed by Doosje *et al.* and introduced earlier in this paper.[41] In the studied structure, the spherical air radius R/D (or inner backbone radius) and channel radius R_c/D were constant. Pockets were then introduced within the backbone as observed in inverse shell opals and non-close-packed inverse shell opals. Indeed, as the backbone outer radius R_{shell}/D is decreased in the Doosje replica, air pockets are introduced within the backbone and grow to form air lattices, as shown in Fig. 1. As defined in Fig. 10, the air lattices are introduced as a function of backbone outer radius R_{shell}/D for values ranging from 0.5 to 0.707, where D is the sphere diameter.

Figure 11(a) shows the evolution of the normalized frequencies of the upper edge of the eighth band and lower edge of the ninth band as a function of the coated sphere radius, R_{shell}/D, for values ranging from 0.54 to 0.707. Additionally, Fig. 11(b) presents the PBG width as a function of the backbone outer radius R_{shell}/D obtained from Fig. 11(a). As shown in Fig. 11(a), the lower W band and upper X band are strongly dependent on structural changes in the air lattices within the backbone, whereas the upper W band showed little dependence on the outer radius. For low infiltration values, the tetrahedral and octahedral air pockets are interconnected by large tubes preventing the occurrence of a PBG. The direct gap opens for $R_{\mathrm{shell}}/D \sim 0.555$, whereas the tetrahedral and octahedral air pockets become connected by thin tubes, as shown in Fig. 1(a). As the outer radius increases; consequently the dielectric volume increases, and the lower edge of the PBG (eighth band at the W point) decreases in frequency but at a lower rate than the upper edge. Hence, the direct $W-W$ PBG width increases accordingly. The tetrahedral air sites eventually vanish, destroying the connectivity between the octahedral and tetrahedral sites. It follows electromagnetic power is transferred from the air domains into the backbone tetrahedral sites. Then, a direct/indirect PBG transition is observed and for further increase of the outer radius, the PBG becomes indirect. As the structure approaches the direct/indirect PBG transition ($R_{\mathrm{shell}}/D \sim 0.66$), the frequency of the upper band at the X point is abruptly pulled down to cross the ninth band at the W point. This is because as the backbone thickness grows, the dielectric/air periodicity of the structure with respect to the X direction is strongly affected by the vanishing of the tetrahedral and octahedral air sites in the backbone. A slight increase in the infiltration promotes a large transfer of the electromagnetic field power density to the backbone. As a consequence, this band gradually transitions from an air band into a dielectric band. Electromagnetic field redistribution is accelerated as the octahedral air sites disappear, thus reducing the indirect gap. Therefore, for a structure presenting no air pockets in the backbone, the indirect gap is minimum.

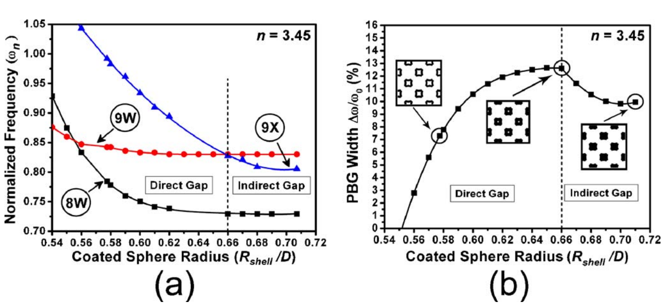

FIG. 11. (Color online) (a) Evolution of the PBG edges: eighth band at the W point and ninth band at the W and X points as a function of coated sphere radius R_{shell}/D. (b) Evolution of the PBG width ($\Delta\omega/\omega_0$ in percent) as a function of coated sphere radius or backbone outer radius R_{shell}/D, where D is the sphere diameter, and for values ranging from 0.5 to 0.707 for high index tube-like non-close-packed inverse shell opals, where $R/D=0.4527$ and $R_c/D=0.1802$.

When no air pockets are present within the backbone, the structure is an exact replica of Doosje's optimized structure, which gives a PBG width of $\sim 10\%$. As the air lattice grows within the backbone forming octahedral air pockets, the indirect $W-X$ PBG width increases to reach a maximum value of 12.5% for $R_{\mathrm{shell}}/D=0.66$, at which point the W and X points at the ninth band cross. Further reduction of the outer radius yields tetrahedral air sites and the direct $W-W$ PBG width decreases. The tetrahedral and octahedral air pockets eventually interconnect to form a true air network embedded into the backbone, and the resulting structure finally loses its complete PBG. For $R_{\mathrm{shell}}/D=0.5775$, the maximum infiltration limit allowed in opal-based structures, the predicted PBG width is 7.2%, close to the value exhibited by structure 7, whereas in contrast a conventional inverse shell opal presenting the equivalent air network only exhibits a PBG width of $\sim 2.5\%$.[13,14]

We have also computed the RIR for different tube-like non-close-packed inverse opals: the original Doosje structure $R_{\mathrm{shell}}/D=0.707$, the optimized inverse shell structure that forms octahedral air pockets only ($R_{\mathrm{shell}}/D=0.66$) and the inverse shell structure incorporating both tetrahedral and octahedral air pockets $R_{\mathrm{shell}}/D=0.5775$. Figure 12 shows the evolution of the PBG width as a function of refractive index for values ranging from 2.4 to 4.0. These data show that a

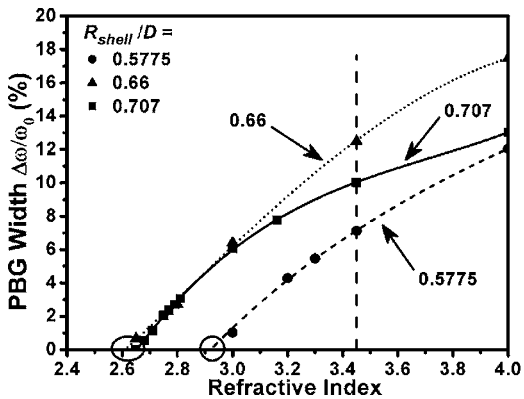

FIG. 12. Evolution of the PBG width ($\Delta\omega/\omega_0$ in percent) as a function of refractive index for values ranging from 2.4 to 4.0 for high index tube-like non-close-packed inverse shell structures with outer backbone radii of $R_{\rm shell}/D$=0.5775, 0.66, and 0.707, respectively.

RIR of 2.65 is predicted in the original structure $R_{\rm shell}/D=0.707$, while a complete PBG is observed for values as low as 2.6 in the optimized non-close-packed inverse shell ($R_{\rm shell}/D$=0.66). Additionally, a RIR of 2.9 is required to open a PBG in the inverse structure, where $R_{\rm shell}/D=0.5775$, compared to 3.3 in similar inverse shell opals. Our calculations also show that for these modified Doosje structures, the RIR properties are very similar to those identified for non-close-packed inverse shell structures fabricated using a sacrificial-layer technique.

V. CONCLUSIONS

In this work, a realistic approach is provided to identify PBG properties in structurally modified non-close-packed inverse opals. An advanced dielectric function was presented to model the complex dielectric nature of experimentally achievable non-close-packed inverse structures. In this scenario, the original template is modified using conformal sacrificial layers and complex hyperboloid air channels are formed as a consequence of a conformal backfilling technique. The conformal sacrificial layers add unprecedented flexibility to selectively modifying the original template and demonstrate that this technique allows structural manipulations of nanoscale architectures. The effect of the structural design and identification of the mechanisms responsible for the formation of the complete PBG were also studied. Using conformally backfilled layers deposited onto modified templates, it was shown that selective modifications of the dielectric/air network topology and filling fraction yield better PBG properties: larger PBG widths and a reduced RIR for opening a PBG, compared to conventional inverse shell opals. In particular, it was emphasized in this work that the conformal deposition of thick sacrificial layers, resulting in a thin 3D-scaffold yields the best PBG properties when appropriately conformally backfilled. An experimentally achievable high index non-close-packed inverse shell structure fabricated using a $R_{\rm SL}/D$=0.5577 sacrificial-shell radius (corresponds to 81.3% infiltration of the air voids), a $R_{\rm shell}/D$=0.5775 backbone outer radius (86% infiltration of the air voids) and a conformally backfilled thickness of $t_{\rm BF}/D$=0.083, is predicted to exhibit a 7.2% PBG width and RIR of 2.9 compared to a conventional inverse shell opal (~2.5% and RIR of 3.3), and will be experimentally investigated in a future work. Furthermore, the introduction of small air pockets within the backbone are theoretically predicted to produce the highest projected PBG width of ~14.2% and a reduced RIR of 2.65 in an optimized inverse shell structure, although at present, fabrication routes for this structure have yet to be developed. The tube-like Doosje model, in which air pockets were introduced, was found to exhibit similar RIR values and large PBG widths, although equivalent practical structures have not yet been made. In contrast, a fully infiltrated non-close-packed inverse shell structure exhibiting a 9.83% PBG width and 2.65 RIR was predicted. It follows that the development of fabrication techniques resulting in fully infiltrated non-close-packed inverse structures by conformal sacrificial-layer/backfilling and sol/gel processes potentially enable PBG materials operating in the visible with lower refractive index materials ($n \geq 2.65$).

ACKNOWLEDGMENTS

This work was supported by the U.S. Army Research Office under MURI Contract DAAD19–01–1-0606. We thank E. Graugnard, J. S. King, and C. Neff for their many fruitful interactions and discussions.

[1]E. Yablonovitch, Phys. Rev. Lett. **58**, 2059 (1987).
[2]S. John, Phys. Rev. Lett. **58**, 2486 (1987).
[3]R. D. Meade, K. D. Brommer, A. M. Rappe, and J. D. Joannopoulos, Phys. Rev. B **44**, 13772 (1991).
[4]J. D. Joannopoulos, P. R. Villeneuve, and S. Fan, Nature (London) **386**, 143 (1997).
[5]J. P. Dowling and C. M. Bowden, J. Mod. Opt. **41**, 345 (1994).
[6]S.-Y. Lin, V. M. Hietala, L. Wang, and E. D. Jones, Opt. Lett. **21**, 1771 (1996).
[7]H. Kosaka, T. Kawashima, A. Tomita, M. Notomi, T. Tamamura, T. Sato, and S. Kawakami, Phys. Rev. B **58**, R10096 (1998).
[8]D. Scrymgeour, N. Malkova, S. Kim, and V. Gopalan, Appl. Phys. Lett. **82**, 3176 (2003).
[9]M. Boroditsky, R. Vrijen, T. F. Krauss, R. Coccioli, R. Bhat, and, E. Yablonovitch, J. Lightwave Technol. **17**, 2096 (1999).
[10]S. E. Barkou, J. Broeng, and A. Bjarklev, Opt. Lett. **24**, 46 (1999).
[11]K. M. Ho, C. T. Chan, and C. M. Soukoulis, Phys. Rev. Lett. **65**, 3152 (1990).
[12]C. T. Chan, Q. L. Yu, and K. M. Ho, Phys. Rev. B **51**, 16635 (1995).
[13]K. Busch and S. John, Phys. Rev. E **58**, 3896 (1998).
[14]S. John and K. Busch, J. Lightwave Technol. **17**, 1931 (1999).
[15]C. T. Chan, S. Datta, K. M. Ho, and C. M. Soukoulis, Phys. Rev. B **50**, 1988 (1994).
[16]S. G. Johnson and J. D. Joannopoulos, Opt. Express **8**, 173 (2001).
[17]S. Noda, K. Tomoda, N. Yamamoto, and A. Chutinan, Science **289**, 604 (2000).
[18]Y. Akahane, T. Asano, B. S. Song, and S. Noda, Opt. Express **13**, 1202 (2005).
[19]A. Blanco, E. Chomski, S. Grabtchak, M. Ibisate, S. John, S. W. Leonard, C. López, F. Meseguer, H. Míguez, J. P. Mondla, G. Ozin, O. Toader, and H. M. van Driel, Nature (London) **405**, 437 (2000).
[20]E. Yablonovitch, T. J. Gmitter, and K. M. Leung, Phys. Rev. Lett. **67**, 2295 (1991).
[21]K. M. Ho, C. T. Chan, C. M. Soukoulis, R. Biswas, and M. Sigalas, Solid State Commun. **89**, 413 (1994).
[22]P. N. Pusey, *Liquids, Freezing and Glass Transition* (Elsevier, New York, 1990).
[23]A. A. Chabanov, Y. Jun, and D. J. Norris, Appl. Phys. Lett. **84**, 3573 (2004).
[24]W. L. Vos, M. Megens, C. M. V. Kats, and P. Bosecke, J. Phys. Condens. Matter **8**, 9503 (1996).

[25] H. S. Sözüer, J. W. Haus, and R. Inguva, Phys. Rev. B **45**, 13962 (1992).
[26] A. Rugge, J. S. Becker, R. G. Gordon, and S. H. Tolbert, Nano Lett. **3**, 1293 (2003).
[27] J. S. King, C. W. Neff, C. J. Summers, W. Park, S. Blomquist, E. Forsythe, and D. Morton, Appl. Phys. Lett. **83**, 2566 (2003).
[28] J. S. King, D. Heineman, E. Graugnard, and C. J. Summers, Appl. Surf. Sci. **244**, 511 (2005).
[29] J. S. King, E. Graugnard, and C. J. Summers, Adv. Mater. (Weinheim, Ger.) **17**, 1010 (2005).
[30] H. Míguez, E. Chomski, F. García-Santamaría, M. Ibisate, S. John, C. López, F. Meseguer, J. P. Mondía, G. A. Ozin, O. Toader, and H. M. van Driel, Adv. Mater. (Weinheim, Ger.) **13**, 1634 (2001).
[31] H. Míguez, N. Tétreault, S. M. Yang, V. Kitaev, and G. A. Ozin, Adv. Mater. (Weinheim, Ger.) **15**, 597 (2003).
[32] F. García-Santamaría, M. Ibisate, I. Rodríguez, F. Meseguer, and C. López, Adv. Mater. (Weinheim, Ger.) **15**, 788 (2003).
[33] B. T. Holland, C. F. Blanford, and A. Stein, Science **281**, 538 (1998).
[34] I. Soten, H. Míguez, S. M. Yang, S. Petrov, N. Coombs, N. Tétreault, N. Matsuura, H. E. Ruda, and G. A. Ozin, Adv. Funct. Mater. **12**, 71 (2002).
[35] P. V. Braun, R. W. Zehner, C. A. White, M. K. Weldon, C. Kloc, S. S. Patel, and P. Wiltzius, Adv. Mater. (Weinheim, Ger.) **13**, 721 (2001).
[36] J. E. G. J. Wijnhoven and W. L. Vos, Science **281**, 802 (1998).
[37] V. F. Kozhevnikov, M. Diwekar, V. P. Kamaev, J. Shi, and Z. V. Vardeny, Physica B **338**, 159 (2003).
[38] V. N. Astratov, A. M. Adawi, M. S. Skolnick, V. K. Tikhomorov, V. Lyubin, D. G. Lidzey, M. Ariu, and A. L. Reynolds, Appl. Phys. Lett. **78**, 4094 (2001).
[39] T. B. Xu, Z. Y. Cheng, Q. M. Zhang, R. H. Baughman, C. Cui, A. A. Zhakhidov, and J. Su, J. Appl. Phys. **88**, 405 (2000).
[40] D. P. Gaillot, T. Yamashita, and C. J. Summers, Phys. Rev. B **72**, 205109 (2005).
[41] M. Doosje, B. J. Hoenders, and J. Knoester, J. Opt. Soc. Am. B **17**, 600 (2000).
[42] F. García-Santamaría, H. T. Miyasaki, A. Urquía, M. Isabate, M. Belmonte, N. Shiniya, F. Meseguer, and C. López, Adv. Mater. (Weinheim, Ger.) **14**, 1144 (2002).
[43] R. Fenollosa and F. Meseguer, Adv. Mater. (Weinheim, Ger.) **15**, 1282 (2003).
[44] F. Meseguer and R. Fenollosa, J. Mater. Chem. **15**, 4577 (2005).
[45] J. S. King, D. P. Gaillot, E. Graugnard, and C. J. Summers, Adv. Mater. (Weinheim, Ger.) **18**, 1063 (2006).
[46] E. Graugnard, J. S. King, D. P. Gaillot, and C. J. Summers, Adv. Funct. Mater. **16**, 1187 (2006).
[47] K. S. Yee, IEEE Trans. Antennas Propag. **AP-14**, 302 (1966).